JOURNAL OF GUIDANCE, CONTROL, AND DYNAMICS
Vol. 18, No. 3, May–June 1995

Approximate Altitude Transitions for High-Speed Aircraft

M. D. Ardema*
Santa Clara University, Santa Clara, California 95053
J. V. Bowles† and E. J. Terjesen‡
NASA Ames Research Center, Moffett Field, California 94035
and
T. Whittaker§
Sterling Software, Moffett Field, California 94035

In a previous paper, a near-optimal guidance law for the ascent trajectory from Earth surface to Earth orbit of a hypersonic, dual-mode propulsion, lifting vehicle was derived. The energy-state approximation was used to determine the near-optimal flight path and the operation of the propulsion system. In this paper, the problem of the instantaneous altitude transitions that occur in energy-state approximation is addressed. The approach is to model the transitions as a sequence of two load factor-bounded paths (either climb-dive or dive-climb). The precise location of the transition is determined from analysis of the boundary-layer equations associated with the energy-state dynamic model.

Introduction

OVER the past seven years, interest in hypersonic, air-breathing aircraft has revived. Missions being studied include space transportation and long distance commercial travel. The vehicles being considered have scramjet propulsion systems augmented by other propulsion modes for low-speed and, possibly, orbital flight.

One feature of a single-stage-to-orbit (SSTO) vehicle is its low payload-to-gross weight fraction. This means that vehicle performance is extremely sensitive to perturbations in vehicle design and operation. In particular, it is essential to optimize the flight path and the operation of the propulsion system to the extent possible in order to attain adequate mission performance and to do this for every competing design under consideration. Although there are well-developed numerical methods for trajectory optimization of point-mass vehicle models, these methods are too expensive computationally and not robust enough to use at the conceptual design stage, in which many hundreds of vehicles must be evaluated and compared on a consistent basis.

Beginning in about 1965, NASA Ames Research Center has developed the hypersonic vehicle synthesis code HAVOC.[1,2] In HAVOC, the vehicle is defined by a geometry database. Other program elements, such as aerodynamics, propulsion, and structures, use this data to make detailed computations of vehicle performance. An important feature of HAVOC is that it may be used iteratively to compute "closed" vehicles, that is, vehicles that meet prespecified requirements of both payload mass and payload volume. Figure 1 shows a typical hypersonic vehicle configuration.

In the past, the trajectory module in HAVOC has been a path-following routine: a flight path is determined external to the synthesis code, perhaps by a numerical optimization, and then inserted into the module. This is undesirable because it is not easily responsive to changes in vehicle design and other characteristics.

In Ref. 3, a guidance law based on the energy-state dynamic model was developed. This dynamic model has been used successfully many times to obtain effective guidance laws for a wide variety of aircraft and missions.[4–9] The key idea is to introduce the total mechanical energy as a state variable and then to neglect all other dynamics. When flight-path optimization is done with this model, simple rules for the optimal path and for the optimal operation of the propulsion system are obtained. In the trajectory module in HAVOC, the guidance law is used to integrate the full point-mass equations of motion. References 8 and 9 also develop energy-state guidance laws for hypersonic aircraft and obtain results similar to Ref. 3.

It is well-known that energy-state optimal trajectories typically feature instantaneous transitions in altitude and velocity at constant energy. These jumps are, of course, unrealistic and may cause significant error. Previous analyses of these transitions have used singular perturbation concepts.[10–13] The equations of motion are formulated as a singularly perturbed system such that the energy-state model emerges as the reduced solution (small parameter set to zero). The boundary-layer equations are then used to model the transitions. In Refs. 10 and 11, simplifications are made such that the transitions can be studied analytically. In Ref. 12, the solution of the transition equations is sought such that the weighted sum of the squares of the errors between the initial and final conditions and the corresponding reduced solution values is a minimum. Ad hoc engineering approaches to transition layers are adopted in Refs. 14 and 15.

The approach adopted here is based on Ref. 13. In that reference, the transition is modeled as two boundary layers back-to-back, one in backward time and one in forward time. In Ref. 13, the lift history is determined by solving the two-point boundary-value problem (2PBVP) resulting from the necessary conditions for optimal control. Because solving a 2PBVP is not practical in a vehicle synthesis code such as HAVOC, in this paper the transition layer lift history is approximated by two constant load factor paths. The transonic transition will be used as an example in numerical results.

Singular Perturbation Formulation and Review of Energy-State Guidance

The derivation begins with the singularly perturbed equations of motion of a point-mass airplane with the following assumptions: 1) The aircraft flies in a great circle about a spherical, rotating Earth (terms in the square of the Earth's rotational speed are neglected). 2) The great circle flight path is maintained by side slipping the vehicle to obtain a component of thrust perpendicular to the flight plane (the effect of side slip on drag is ignored). 3) The lift vector

Received Dec. 3, 1993; revision received Nov. 20, 1994; accepted for publication Dec. 22, 1994.

*Professor and Chairman, Department of Mechanical Engineering. Associate Fellow AIAA.
†Aerospace Engineer, Systems Analysis Branch. Member AIAA.
‡Engineering Assistant; also Graduate Student, Department of Mechanical Engineering, Santa Clara University (deceased). Student Member AIAA.
§Programmer/Analyst, Computational Sciences.

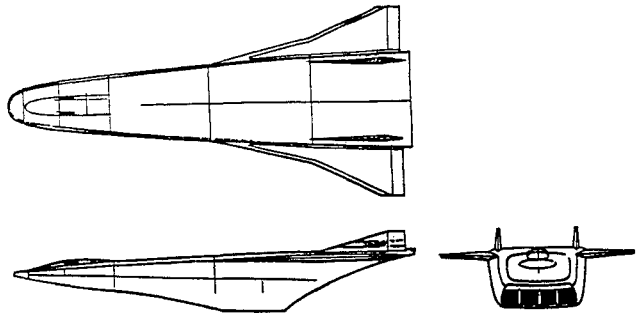

Fig. 1 Hypersonic aircraft configuration.

is in the flight plane (zero bank angle). 4) There are zero ambient winds. Under these assumptions, the equations are

$$\begin{aligned} \varepsilon_2 \dot{h} &= V \sin\gamma \\ \dot{E} &= (V/mg_s)(T_V - D) = P \\ \dot{m} &= -\beta \\ \varepsilon_1\varepsilon_2\dot{\gamma} &= \frac{V\cos\gamma}{R+h} - \frac{g\cos\gamma}{V} + \frac{T_\gamma + L}{mV} + 2\Omega_\gamma \end{aligned} \tag{1}$$

In these equations, the state variables are the height above the surface of the Earth h, the total mechanical energy E, the vehicle mass m, and the flight-path angle γ. T_V, T_γ, and T_S are the components of thrust along the velocity vector, perpendicular to the velocity vector and in the great circle, and perpendicular to the great circle, respectively; D is drag; R is the radius of the Earth; g_s is the sea level gravitational acceleration; g is the local gravitational acceleration; and Ω_γ is the γ component of the Earth rotation (Coriolis) term, which depends on instantaneous heading and latitude, as well as on Earth rotation rate. The control variables are the angle of attack α and the engine fuel mass flow rate β. Energy, altitude, and velocity are related by the equation

$$E = [hR/(R+h)] + (1/2g_s)V^2 \tag{2}$$

These equations, with $\varepsilon_1 = 0$ and $\varepsilon_2 = 1$, are integrated in the HAVOC code.

The energy state model is obtained by setting $\varepsilon_1 = 1$ and $\varepsilon_2 = 0$ in Eq. (1), resulting in the two state equations $\dot{E} = P$ and $\dot{m} = -\beta$. To be useful, these equations must be dependent only on altitude h and speed V. In general, however, P also depends on angle of attack α, which couples the energy state equation to the other equations in Eq. (1). In subsonic aircraft, this dependency is generally eliminated by assuming that the thrust vector is aligned with the velocity vector and by evaluating drag with lift equalized to weight. For hypersonic aircraft, however, the dependence of P on α is quite complicated and significant. First, the thrust vector is considerably offset from the velocity vector, and it is only the component along the velocity vector that affects P. Second, the air-breathing engine thrust magnitude also depends on α because α affects the mass capture area and thus the airflow into the engine. Finally, if both a rocket engine and an air-breathing engine are operating simultaneously, the rocket throttle setting affects air-breather thrust through α effects. All of these effects are accounted for in the present paper, and, consistent with energy-state approximation, the value of α used to evaluate P is determined by enforcing equilibrium in the airplane plane of symmetry in a direction perpendicular to the velocity vector.

For a SSTO mission with a hypersonic aircraft, what is desired is a trajectory that gives the minimum gross takeoff weight vehicle to put a given payload mass and volume in orbit. Because liquid hydrogen fueled aircraft have relatively low-gross densities and correspondingly high-surface area to gross weight ratios, they are very sensitive to perturbations in volume as well as in mass, and it is, therefore, necessary to minimize a weighted sum of fuel mass and volume. Thus, the cost functional is taken as

$$\psi = -\int_{m_0}^{mf} \mathrm{d}m - K\int_{v_{f_0}}^{v_{f_f}} \mathrm{d}v_f \tag{3}$$

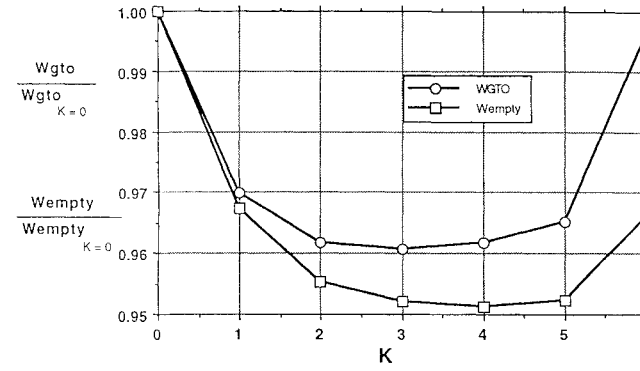

Fig. 2 Effect of weighting parameter K.

where v_f is the fuel volume, and $K \in [0, \infty)$ is a weighting parameter.

The optimal value of K is determined numerically by computing closed vehicles for a range of values of K, that is, iteratively exercising the HAVOC code to obtain the gross takeoff weight and volume required to put a specified payload weight and volume in a specified orbit. The result for a typical SSTO is shown in Fig. 2. It is seen that a value of $K = 3$ lbs/ft^3 gives very nearly a minimum of both takeoff weight and empty weight, and this value will be used throughout the rest of the paper. The figure shows that use of the optimally weighted cost functional saves 4% in gross weight and 5% in empty weight, relative to minimizing fuel weight only.

Another feature of SSTO aircraft that needs to be taken into account is that they have two (or more) independent propulsion modes. Thus, the total thrust (along the velocity vector) and fuel flow rates are

$$\begin{aligned} T_V &= f_V[\pi_a T_{Ma}\cos(\alpha + \zeta_a) + \pi_r T_{Mr}\cos(\alpha + \zeta_r)] \\ \beta &= C_a\pi_a T_{Ma} + C_r\pi_r T_{Mr} \end{aligned} \tag{4}$$

where $\pi \in [0, 1]$ is throttle setting, T_M maximum thrust, ζ thrust offset angle, C thrust specific fuel consumption, and f_V a parameter to account for the fact that the thrust and velocity vectors are not collinear. The subscripts a and r refer to the two propulsion modes, later to be identified as air breather and rocket, respectively.

The quantity to be maximized at each energy level under the energy-state assumption is then

$$\frac{P}{\Phi} = \frac{V(f_1 + f_2 - D)}{mg_s(C_1 + C_2)} \tag{5}$$

where

$$\begin{aligned} \Phi &= \dot{\psi} \\ f_1 &= f_V\pi_a T_{Ma}\cos(\alpha + \zeta_a) \\ f_2 &= f_V\pi_r T_{Mr}\cos(\alpha + \zeta_r) \\ C_1 &= C_a\pi_a T_{Ma}[K(\rho_a - 1) + 1]/\rho_a \\ C_2 &= C_r\pi_r T_{Mr}[K(\rho_r - 1) + 1]/\rho_r \end{aligned} \tag{6}$$

and ρ_a and ρ_r are the net densities of the airbreathing and the rocket fuel, respectively. The angle of attack to be used in computing P/Φ is determined from

$$0 = \frac{V}{R+h} - \frac{g}{V} + \frac{T_\gamma + L}{mV} + 2\Omega_\gamma \tag{7}$$

The controls are now $u = (\pi_a, \pi_r, V)^T$. The constraints on these controls will now be discussed. Figure 3 shows the constraints on the throttle settings. Figure 3a shows equivalence ratio e as a function of freestream Mach number M for the air-breathing engine. Equivalence ratio is defined as the ratio of actual fuel flow to the fuel flow for stoichiometric combustion. The resultant thrust from the air-breathing propulsion system is then the product of four variables: the equivalence ratio, the stoichiometric fuel-to-air ratio, the air mass flow rate captured by the engine, and the cycle specific impulse (pounds of thrust per pound of fuel flow). The stoichiometric

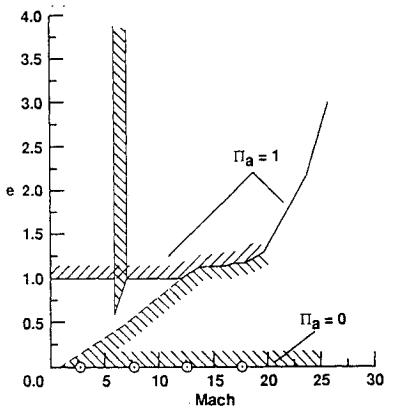

a) Air breather

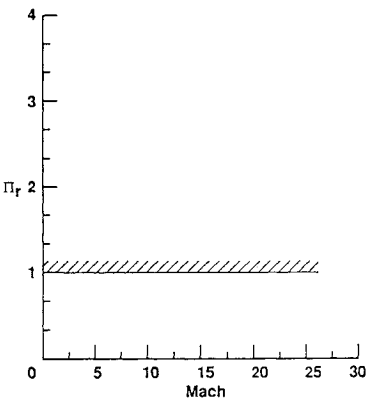

b) Rocket

Fig. 3 Constraints on throttle controls.

fuel-to-air ratio is a function of the fuel type. The air capture rate is computed as a function of Mach number, freestream dynamic pressure, angle of attack, and forebody/cowl geometry. The specific impulse is a strong function of freestream Mach number and engine equivalence ratio and only moderately dependent on dynamic pressure and angle of attack. In this analysis, the specific impulse is modeled only as a function of Mach number at full throttle setting ($\pi_a = 1$). This approximation will give acceptable engineering modeling of the air-breather performance. The equivalence ratio model is presented next.

For Mach numbers less than 6.0, the engine operates in the ramjet mode. In this mode, the engine can be operated over a wide range of equivalence ratios, with a lower bound constrained by required engine/airframe cooling fuel flow rate which, in general, is a function of Mach number and altitude (i.e., dynamic pressure). Since if there are no considerations other than combustion efficiency it is not optimum to have $e > 1$, the upper limit $e \leq 1$ is imposed. At Mach 6, the start of the supersonic combustion ramjet mode, there is a pronounced reduction in the allowable engine equivalence ratio due to engine operating limits of thermal choke/burner exit Mach number for the limited variable geometry scramjet engines. The net result is a sharp dip in the upper bound for the air-breathing engine to limit heat release in the combustor, as shown in Fig. 3a. As the Mach number is increased in the scramjet mode, this constraint vanishes and the engine is allowed to again burn stoichiometrically. Starting at approximately Mach 12, the airframe/engine cooling requirement determines the required engine fuel flow rate and, hence, the equivalence ratio must be greater than the stoichiometric value ($e = 1$). In general, the engine equivalence ratio required for cooling will be a function of Mach number and dynamic pressure, with a mild dependence on angle of attack. In this analysis, the angle-of-attack dependence is ignored, and the cooling equivalence ratio was computed at the resultant dynamic pressure constrained by forebody compression ramp surface equilibrium radiation temperature limit, which turns out to be the optimal trajectory in the scramjet operating mode.

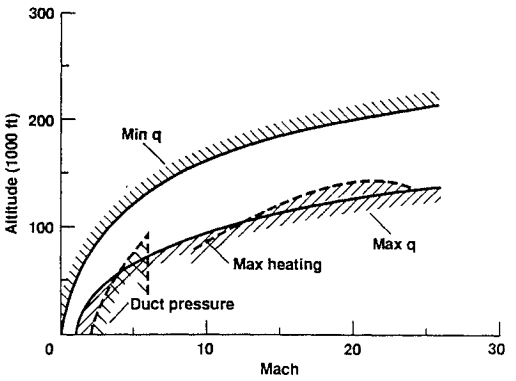

Fig. 4 Constraints on velocity control.

One option always is to turn the air-breathing engine completely off. This is represented by the lower bound of $\pi_a = 0$. For this option, the scramjet duct is closed off using the variable cowl geometry and no engine cooling fuel flow is required, with the external cowl surface radiatively cooled. All of these constraints and requirements define the set of admissible controls and result in the definitions of $\pi_a = 1$ and $\pi_a = 0$, shown in Fig. 3a. The bounds on the throttle setting of the rocket engine, Fig. 3b, are straightforward.

The bounds on V are shown in Fig. 4. The four constraints are 1) a minimum dynamic pressure ($q_{\min}$), 2) a maximum dynamic pressure ($q_{\max}$), 3) a duct pressure limit, and 4) an aerodynamic heating limit on the airframe structure. These constraints define V_m and V_M, the minimum and maximum values of V, as a function of M.

The maximization of Eq. (5) with respect to π_a, π_r, and V, subject to the control constraints depicted in Figs. 3 and 4, gives the following guidance law for the optimal controls[3,8,9]:

$$V^* = \arg\max_{V_m \leq V \leq V_M} \left(\frac{P}{\Phi}\right)_{\pi_a^*, \pi_r^*, E} \tag{8}$$

$$\left.\begin{aligned}
&\text{If} \quad \frac{C_a^* \rho_r}{C_r^* \rho_a} \geq \frac{K(\rho_r - 1) + 1}{K(\rho_a - 1) + 1} \\
&\text{then} \\
&\qquad \pi_r^* = 1 \\
&\qquad \pi_a^* = \begin{cases} 0 & \text{if } 1 - \dfrac{D^*}{T_{Mr}^*} > \dfrac{C_r^* \rho_a [K(\rho_r - 1) + 1]}{C_a^* \rho_r [K(\rho_a - 1) + 1]} \\ 1 & \text{otherwise} \end{cases} \\
&\text{If} \quad \frac{C_a^* \rho_r}{C_r^* \rho_a} < \frac{K(\rho_r - 1) + 1}{K(\rho_a - 1) + 1} \\
&\text{then} \\
&\qquad \pi_a^* = 1 \\
&\qquad \pi_r^* = \begin{cases} 0 & \text{if } 1 - \dfrac{D^*}{T_{Ma}^*} > \dfrac{C_a^* \rho_r [K(\rho_a - 1) + 1]}{C_r^* \rho_a [K(\rho_r - 1) + 1]} \\ 1 & \text{otherwise} \end{cases}
\end{aligned}\right\} \tag{9}$$

Because of the great complexity of the engine, and especially the variable engine geometry features, the variation of P/Φ with V is quite complex. A section of this function in the transonic region for the aircraft depicted in Fig. 2 is shown in Fig. 5. The black line shows the energy-climb path determined from Eqs. (8) and (9).

Altitude Transitions

Constant energy transitions occur when the altitude (or, equivalently the velocity) that maximizes P/Φ changes instantaneously at some level of E, say $\bar{E}$, at some time, say $\bar{t}$. A typical situation is depicted in Fig. 6. For $E < \bar{E}$, the higher relative maximum of P/Φ is the global maximum, whereas for $E > \bar{E}$ the lower maximum is the

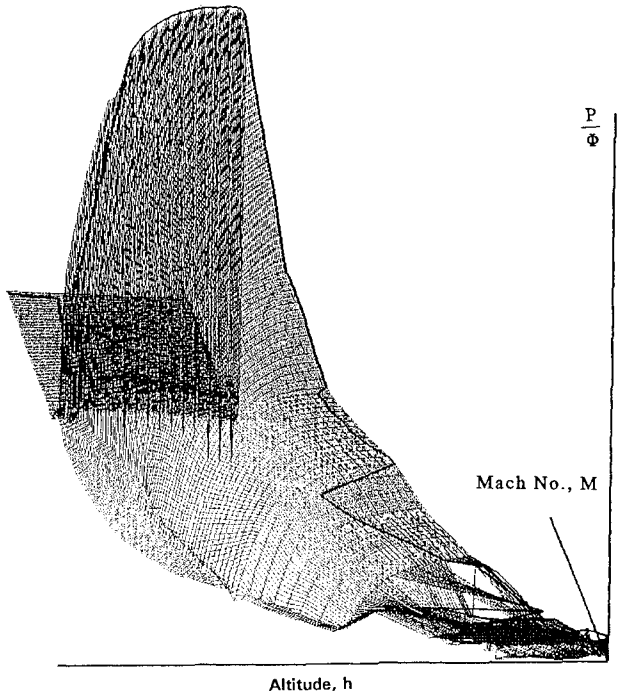

Fig. 5 Cost function in the transonic region.

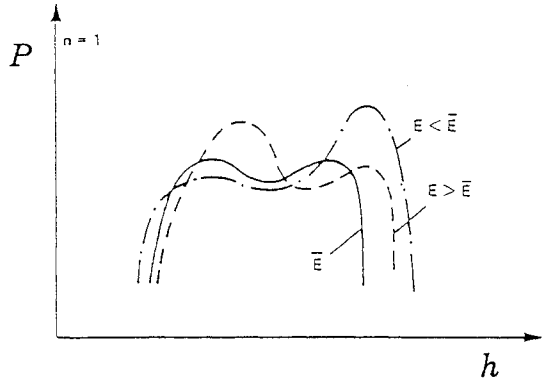

Fig. 6 Variation of cost function with altitude near an energy transition.

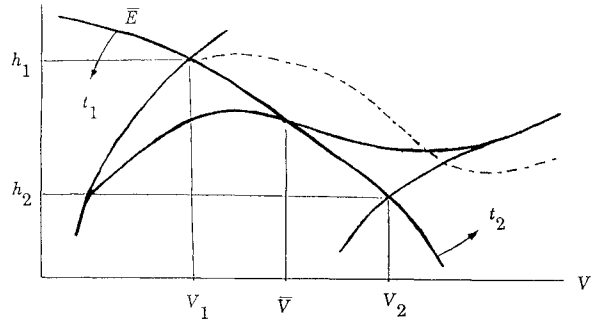

Fig. 7 Sketch of energy transition.

global one. At $\bar{E}$, therefore, there is a jump in the energy-climb path from higher altitude and lower speed to lower altitude and higher speed (Fig. 7). Such transitions can also occur from lower to higher altitudes, and either to or from either upper or lower flight envelope constraints.

One way of approximating optimal transitions is to begin flying a minimum fixed load factor flight path when a jump is detected (for the case of a jump from a higher to lower altitude) and then switch to maximum fixed load factor when the new branch is crossed; this is the dotted path in Fig. 7. There are two undesirable features of this approach. First, the transition is done too late, resulting in a loss of optimality. Second, the transition overshoots the new branch; this also results in a loss of optimality and may be unacceptable if the new branch lies on a flight-path constraint.

In Ref. 13, transition layers are treated as two boundary layers, one in backward time and one in forward time. Each layer is matched with its appropriate energy-climb path branch and with the other boundary layer at $\bar{E}$. The layers are then used to form a uniformly valid composite solution. The composite solution for a dive transition consists of a pushover (load factor n less than one) followed by a pullup (n greater than one); for a climb transition, this sequence is reversed.

The transition load factor history in Ref. 13 was determined from solving the 2PBVP arising from the necessary conditions of optimal control. Since this is impractical in a vehicle synthesis code, in the present application the load factor during the two boundary-layer motions are taken to be constants, n_1 for $t < \bar{t}$ and n_2 for $t > \bar{t}$. Then, for a dive transition, $n_1 < 1 < n_2$, and for a climb transition, $n_1 > 1 > n_2$. Boundary-layer analysis will now be used to determine $\bar{V}$, the velocity at which the transition layer passes through $\bar{E}$.

Making the transformations

$$t_1 = (\bar{t} - t)/\varepsilon_2, \qquad t_2 = (t - \bar{t})/\varepsilon_2 \tag{10}$$

in Eq. (1) and then setting $\varepsilon_2 = 0$ gives the boundary-layer equations

$$(-1)^i \frac{dh}{dt_i} = V \sin\gamma$$

$$(-1)^i \frac{d\gamma}{dt_i} = \frac{V\cos\gamma}{R+h} - \frac{g\cos\gamma}{V} + \frac{T_\gamma + L}{mV} + 2\Omega_\gamma$$

for $i = 1, 2$, where E and m (the slow variables) are constant, and where V as a function of h and E is given by Eq. (2). A slightly simpler, but equivalent, set of equations may be obtained by differentiating Eq. (2) with respect to time, using the fact that E is a constant, and solving for $\dot{V}$; the result is

$$\begin{aligned} (-1)^i \frac{dV}{dt_i} &= -g\sin\gamma \\ (-1)^i \frac{d\gamma}{dt_i} &= \frac{V\cos\gamma}{R+h} - \frac{g\cos\gamma}{V} + \frac{T_\gamma + L}{mV} + 2\Omega_\gamma \end{aligned} \tag{11}$$

These equations may be integrated in closed form for constant load factor flight if the flight-path angle is taken to be small (consistent with energy-state approximation), and if g and the term $R + h$ are taken as constant during the transition. Using Eq. (2), setting $\sin\gamma = \gamma$ and $\cos\gamma = 1$, and eliminating time from Eq. (11) gives

$$\frac{dV}{d\gamma} = -\frac{g\gamma}{(V/R') - (g/V) + (gn/V) + 2\Omega_\gamma} \tag{12}$$

where $R' = R + h$. Integrating results in

$$-\frac{V^2}{2R'g} - k\ell_n V - \frac{2\Omega_\gamma V}{g} = \frac{1}{2}\gamma^2 + C_i \tag{13}$$

where

$$k = n - 1 \tag{14}$$

The constants of integration C_i are determined by applying boundary and matching conditions. For $i = 1$, we have $t < \bar{t}$, $n = n_1$, and $k = k_1 = n_1 - 1$. As $t_1 \to \infty$, in this boundary layer $\gamma \to \gamma_1$ and $V \to V_1$. (Strictly speaking, the flight-path angle is zero on the energy climb path. The numerical integration, however, provides nonzero values of γ at V_1 and V_2, and, since it is easy to account for this in the boundary-layer solutions, we do so.) From Eq. (11), this gives

$$-\frac{V_1^2}{2R'g} - k_1\ell_n V_1 - \frac{2\Omega_\gamma V_1}{g} = \frac{1}{2}\gamma_1^2 + C_1 \tag{15}$$

Also, as $t_1 \to 0$, $\gamma \to \bar{\gamma}$, and $V \to \bar{V}$; thus,

$$-\frac{\bar{V}^2}{2R'g} - k_1 \ell_n \bar{V} - \frac{2\Omega_\gamma \bar{V}}{g} = \frac{1}{2}\bar{\gamma}^2 + C_1 \tag{16}$$

Eliminating C_1 between these two equations,

$$\frac{1}{2R'g}\left(V_1^2 - \bar{V}^2\right) + \ell_n\left(\frac{V_1}{\bar{V}}\right)^{k_1} = \frac{1}{2}\left(\bar{\gamma}^2 - \gamma_1^2\right) + \frac{2\Omega_\gamma}{g}(\bar{V} - V_1) \tag{17}$$

A similar matching analysis for the other boundary layer, $i = 2$, gives

$$\frac{1}{2R'g}\left(V_2^2 - \bar{V}^2\right) + \ell_n\left(\frac{V_2}{\bar{V}}\right)^{k_2} = \frac{1}{2}\left(\bar{\gamma}^2 - \gamma_2^2\right) + \frac{2\Omega_\gamma}{g}(\bar{V} - V_2) \tag{18}$$

Equations (17) and (18) may now be used to eliminate $\bar{\gamma}$ and obtain an expression giving $\bar{V}$ in terms of the known quantities V_1, V_2, k_1, and k_2; the result is

$$\bar{V} = \left[e^{\frac{V_2^2 - V_1^2}{2R'g}} e^{\frac{2\Omega_\gamma (V_2 - V_1)}{g}} e^{\frac{\gamma_2^2 - \gamma_1^2}{2}} \left(\frac{V_2^{k_2}}{V_1^{k_1}}\right) \right]^{\frac{1}{k_2 - k_1}} \tag{19}$$

The four terms in this equation have the following interpretation. The first term is a correction for Earth curvature (centripetal acceleration), the second is a correction for Earth rotation (Coriolis acceleration), the third is a correction for flight-path angle (longitudinal acceleration), and the fourth is the main term (thrust and lift effects). Although the Earth curvature and rotation corrections are not important for transonic transitions, they will be important for transitions at higher speeds.

Note that for $\gamma_1 = \gamma_2 = 0$, $\Omega_\gamma = 0$ (nonrotating Earth), and $R \to \infty$ (flat Earth), Eq. (19) reduces to

$$\bar{V} = \left(V_2^{n_2 - 1} / V_1^{n_1 - 1}\right)^{[1/(n_2 - n_1)]} \tag{20}$$

Having found $\bar{V}$, the final step is to find the path satisfying Eq. (1) with $\varepsilon_1 = 0$ and $\varepsilon_2 = 1$ that transitions through $\bar{E}$ with speed $\bar{V}$, has $n = n_1$ for $E < \bar{E}$ and $n = n_2$ for $E > \bar{E}$, and meets the two subsonic and supersonic branches of the trajectory smoothly. The best way to do this is a topic under current investigation. For the present paper, the following ad hoc procedure is adopted. When a jump (either dive or climb) is detected in the energy-climb path, V_1 and V_2 are determined and $\bar{V}$ is computed from Eq. (19). A search is then made for the departure point on the $t < \bar{t}$ branch of the energy-climb path such that a constant load factor path with load factor n_1 just passes through $\bar{E}$ with velocity $\bar{V}$. At $\bar{E}$, the load factor is switched to n_2 and a constant load factor path is followed until the $t > \bar{t}$ branch of the energy-climb path can be rejoined without violating load factor limits.

Numerical Results

Because of a sharp increase in drag near Mach 1, many high-performance supersonic aircraft have a dive in their energy-climb paths in the transonic region.[12,13] This is generally true of hypersonic vehicles as well, and this transonic jump will be used to illustrate the transition algorithm developed in the preceding section. The transonic dive depicted in Fig. 5 is shown in the altitude-Mach plane in Fig. 8. As Mach 1 is approached, the energy-climb path begins to rise at nearly constant, slightly subsonic Mach number; then at 43,000-ft altitude it transitions to 3,000 ft and $M = 1.7$ (dynamic pressure limits are ignored for now). Both the subsonic and supersonic portions of the energy-climb path are with only the air-breathing engine on.

Conditions just before and just after the dive and the two specified transition load factors $n_1 = 0.5$ and $n_2 = 2.5$ are used to compute $\bar{V}$ from Eq. (19); this gives approximately $\bar{M} = 1.55$. The path with constant load factor $n_1 = 0.5$ that just passes through $\bar{E}$ with speed $\bar{M}$ was found to start on the energy-climb path at 25,000 ft. At $\bar{E}$, the load factor is switched to $n_2 = 2.5$, and the transition path then eventually joins the energy-climb path at about $M = 2.1$.

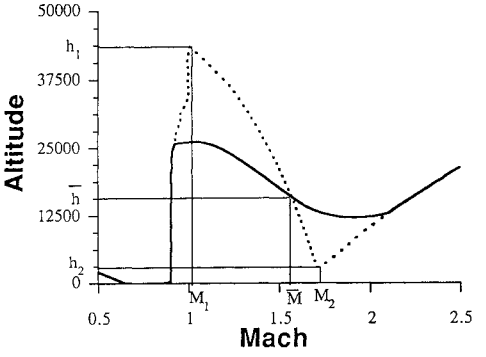

Fig. 8 Transonic transition trajectory: - - -, energy-climb path; ——$N1$ = 0.5, $N2$ = 2.5.

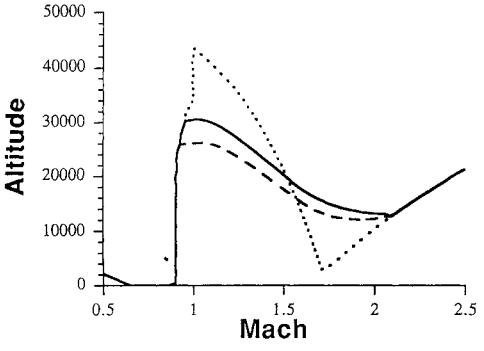

Fig. 9 Comparison of transition trajectories for n_2 = 2.0 and n_2 = 2.5: - - -, energy-climb path; ——, $N1$ = 0.5, $N2$ = 2.0; – – –, $N1$ = 0.5, $N2$ = 2.5.

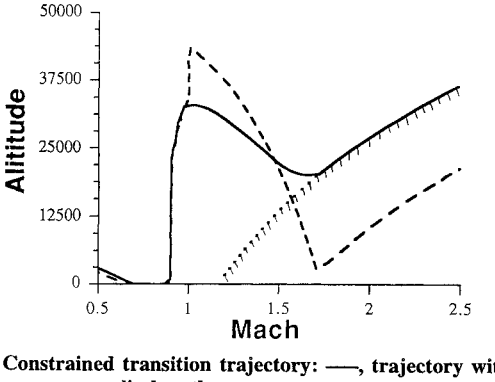

Fig. 10 Constrained transition trajectory: ——, trajectory with constraint; – – –, energy-climb path.

The transition path is obtained by integration of the full equations of motion [Eq. (1)] with $\varepsilon_1 = 0$ and $\varepsilon_2 = 1$.

The two transition load factors, n_1 and n_2, are available as parameters to be chosen to maximize vehicle performance. Figure 9 shows the transonic transition trajectories for both $n_2 = 2.0$ and $n_2 = 2.5$ with $n_1 = 0.5$. The $n_2 = 2.5$ trajectory transitions through $\bar{E}$ lower because the pullup after $\bar{E}$ is steeper than for the $n_2 = 2.0$ path. The $n_2 = 2.5$ trajectory burned 437 lb more fuel than did the $n_2 = 2.0$ trajectory, indicating that the latter is a better choice. Selection of the best values of n_1 and n_2 will take further numerical experimentation.

Portions of hypersonic trajectories typically lie on the path constraints (Fig. 10), and their energy-climb paths jump to and from these constraints. In fact, the high-speed branch of the energy-climb path shown in Figs. 8 and 9 violates the usual maximum dynamic pressure constraint. Because time has been eliminated from the boundary-layer solutions [Eqs. (12–19)], these equations may be used for jumps to and from constraints. Figure 10 shows a 2000-psf dynamic pressure constraint imposed on the trajectory. The quantity V_2 is now the velocity where $\bar{E}$ and the constraint meet. This has the effect of decreasing $\bar{V}$ and, in turn, raising the altitude of the transition path. The figure shows that this results in a path which joins the constraint, indicating success of the method.

Concluding Remarks

The transition between branches of the energy-climb path for hypersonic aircraft have been investigated. Based on previous results, the transitions are modeled as two constant load factor paths. The location of the transition is determined by using singular perturbation methods; two boundary layers are matched at the transition energy to obtain the location of the transition. Numerical examples show the method to be effective.

In Memoriam

The other three authors dedicate this paper to Eric Terjesen, who died June 2, 1994, at the age of 25.

References

[1]Petersen, R. H., Gregory, T. J., and Smith C. L., "Some Comparisons of Turboramjet-Powered Hypersonic Aircraft for Cruise and Boost Missions," *Journal of Aircraft*, Vol. 3, No. 5, 1966, p. 398.

[2]Bowles, J. V., "Ames Conceptual Studies Activities," Proceedings of the Second National Aerospace Plane Symposium, Applied Physics Lab., Laurel, MD, Nov. 1986.

[3]Ardema, M. D., Bowles, J. V., and Whittaker, T., "Optimal Trajectories for Hypersonic Launch Vehicles," *Lecture Notes in Control and Information Sciences*, Vol. 170, edited by J. M. Skowronski, H. Flashner, and R. S. Guttalu, Springer–Verlag, Berlin, 1992, p. 18.

[4]Bryson, A. E., Jr., Desai, M. N., and Hoffman, W. C., "Energy-State Approximation in Performance Optimization of Supersonic Aircraft," *Journal of Aircraft*, Vol. 6, No. 6, 1969, p. 481.

[5]Kelley, H. J., Cliff, E. M., and Weston, A. R., "Energy State Revisited," *Optimal Control Applications and Methods*, Vol. 7, No. 2, 1986, p. 195.

[6]Ardema, M. D., "Solution of Minimum Time-to-Climb Problem by Matched Asymptotic Expansions," *AIAA Journal*, Vol. 14, No. 7, 1976, p. 843.

[7]Kelley, H. J., "Aircraft Maneuver Optimization by Reduced-Order Approximation," *Control and Dynamic Systems*, Vol. 10, edited by C. T. Leondes, Academic, New York, 1973, p. 131.

[8]Van Buren, M. A., and Mease, K. D., "Aerospace Plane Guidance Using Geometric Control Theory," *Proceedings of the 1990 American Control Conf.*, San Diego, CA, May 23–25, 1990.

[9]Corban, J. E., Calise, A. J., and Flandro, G. A.,"Rapid Near-Optimal Aerospace Plane Trajectory Generation and Guidance," *Journal of Guidance, Control, and Dynamics*, Vol. 14, No. 6, 1991, p. 1181.

[10]Breakwell, J. V., "Optimal Flight-Path-Angle Transitions in Minimum-Time Airplane Climbs," *Journal of Aircraft*, Vol. 14, No. 8, 1977, p. 782.

[11]Breakwell, J. V., "More About Flight-Path-Angle Transitions in Optimal Airplane Climbs," *Journal of Guidance and Control*, Vol. 1, No. 3, 1978, p. 205.

[12]Weston, A. R., Cliff, E. M., and Kelley, H. J., "Altitude Transitions in Energy Climbs," *Automatica*, Vol. 19, No. 2, 1983, p. 199.

[13]Ardema, M. D., and Yang, L., "Interior Transition Layers in Flight-Path Optimization," *Journal of Guidance, Control, and Dynamics*, Vol. 11, No. 1, 1988, p. 13.

[14]Shinar, J., and Fainstein, V., "Improved Feedback Algorithms for Optimal Maneuvers in Vertical Plane," AIAA Paper 85-1976, 1985.

[15]Huynh, H. T., and Moreigne, O., "Quasi-Optimal On-Line Guidance Laws for Military Aircraft," AIAA Paper 85-1977, 1985.